The Journal of Supercritical Fluids 133 (2018) 239–252

Contents lists available at ScienceDirect

The Journal of Supercritical Fluids

journal homepage: www.elsevier.com/locate/supflu

Solubility measurement and preparation of nanoparticles of an anticancer drug (Letrozole) using rapid expansion of supercritical solutions with solid cosolvent (RESS-SC)

Gholamhossein Sodeifian[a,b,*], Seyed Ali Sajadian[a,b]

[a] Department of Chemical Engineering, Faculty of Engineering, University of Kashan, Postal Code: 87317-53153, Kashan, Iran
[b] Laboratory of Supercritical Fluids and Nanotechnology, University of Kashan, Postal Code: 87317-53153, Kashan, Iran

GRAPHICAL ABSTRACT

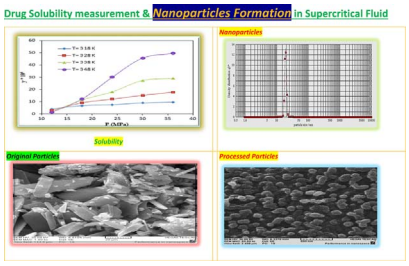

ARTICLE INFO

Keywords:
Anticancer nanoparticles (nanodrug)
Letrozole
RESS-SC
Solubility
Optimization (Taguchi method)

ABSTRACT

A method of rapid expansion of supercritical solutions with solid cosolvent (RESS-SC) was applied, for the first time, to precipitate nanoparticles of Letrozole (LTZ). Solubility of LTZ, as a poorly water-soluble drug, was measured under various conditions in supercritical CO_2 with/without menthol as cosolvent. The solubility of LTZ in ternary system (with solid cosolvent) was increased 7.1 times as large as that of binary system (without solid cosolvent). Then, influences of temperature, pressure, solid cosolvent and spray distance on the size and morphology of the particles were investigated by Taguchi technique. The analysis of variance results showed that, temperature and pressure had the most and least significant impacts on the size-reduction of nanoparticles, respectively. The particles were characterized using SEM, DLS, XRD, FTIR and DSC. Experimental observations revealed that the LTZ particles were nanosized from the original average size of 30 μm to the smallest average size of 19 nm.

1. Introduction

Breast cancer is the most common malignancy and non-cutaneous cancer among women. It is the second leading cause of cancer-related deaths in the United States [1]. Nowadays, representing a new class of agents, aromatase inhibitors are considered as more effective than tamoxifen (cancer drug) in treatment of breast cancer [2]. Letrozole (LTZ) is an oral non-steroidal aromatase inhibitor approved by United States FDA. It has been proposed for adjuvant treatment of hormonally-responsive local or metastatic breast cancer [3,4]. Basically, LTZ decreases the amount of estrogen produced by the body in an attempt to slow down or even stop the growth of some breast tumors that need estrogen to grow. The drug has been also used for postmenopausal women with hormone-dependent breast cancer [5]. Additionally, LTZ is rapidly and completely absorbed from the gastrointestinal tract, with absorption not affected by food.

* Corresponding author at: Department of Chemical Engineering, Faculty of Engineering, University of Kashan, Postal Code: 87317-53153, Kashan, Iran.
E-mail address: sodeifian@kashanu.ac.ir (G. Sodeifian).

http://dx.doi.org/10.1016/j.supflu.2017.10.015
Received 16 August 2017; Received in revised form 18 October 2017; Accepted 18 October 2017
Available online 28 October 2017
0896-8446/

Nomenclature

$a_0 - a_5$	Adjustable parameters of model
AARD	Average absolute relative deviation
a	Empirical parameter
A	Surface area of solute
b	Empirical parameter
C	Concentration of the solute in the bulk
C_s	Concentration of the solute in the diffusion layer
D	Diffusivity
$^{dw}/_{dt}$	Rate of dissolution
f_1	Difference factor
f_2	Similarity factor
k_w	Dissolution rate coefficient
L	Diffusion layer thickness
MS_R	Mean square regression
MS_E	Mean square residual
M_W	Molar mass, kg mol^{-1}
N	Number of data points, dimensionless
P	Pressure
P_{ref}	Reference pressure
Q	Number of independent variables in each equation
R^2	Correlation coefficient
R_j	Dissolved percentage of original sample
SSE	Error sum of squares
SST	Total sum of squares
SSR	Regression sum of squares
T	Temperature, K
T_j	Dissolved percentage of processed sample
y	Mole fraction solubility

Greek symbols

ρ	Density, kg/m^3

Subscripts

1	Solvent (SCF)
2	Solute (Drug)
3	Cosolvent (Menthol)
c	Critical property
cal	Calculated
exp	Experimental
i, j	Component

In the pharmaceutical industry, water-insolubility or poor water-solubility is one of the main barriers against optimal performance of active pharmaceutical ingredients (API). Also, bioavailability of these drugs is limited by their insolubility. Dissolution rate depends on size and size distribution of drug particles and their solubility characteristics. Based on Noyes–Whitney equation, the dissolution rate is improved by maximization of particle's surface area which can be achieved by reducing the particle size [6,7].

$$\frac{dw}{dt} = \frac{DA(C_s - C)}{L} \tag{1}$$

Where $^{dw}/_{dt}$ is the rate of dissolution, A is the surface area of solute, C is the concentration of the solute in the bulk dissolution medium, C_s is the concentration of the solute in the diffusion layer surrounding the solute, D is the diffusivity, and L is the diffusion layer thickness. As a result, bioavailability of the water-insoluble drugs can be raised by decreasing specific surface areas of their particles. Conventionally, several methods have been applied for producing micro and nanoparticles, including milling, grinding, spray drying, and recrystallization from solution [8]. Disadvantages of these techniques include high energy requirement, high solvent consumption, and the need for further purification steps (in some cases). Furthermore, some APIs are unstable under milling conditions, and there are chances that the product is contaminated with solvent during the course of recrystallization process. In contrast, addressing these drawbacks, the so-called supercritical fluid (SCF) technique is an environment-friendly method that is capable of producing micro and nanoparticles of drugs [9,10].

The use of SCF for producing fine particles has increased enormously due to their exceptional properties such as solvent power, high diffusivity and low viscosity. Besides that, purity of products, simplicity of the processes, possibility of producing solid phases with unique morphologies, and mildness of operating conditions make it possible to obtain fine particles with narrow size distribution. Supercritical carbon dioxide (SC-CO_2) is most commonly used as a solvent or anti-solvent for reducing API particles, because of its relatively low critical temperature and moderate critical pressure. Additionally, it is inexpensive, non-toxic, and non-flammable [11–15].

As mentioned, one of alternative ways for improving solubility and dissolution rate of poorly water soluble drugs is represented by SCF technology. In the other words, reduction of API using SCF methods, which go through much simpler steps, can eliminate thermal sensitivity and impurity contamination problems faced in traditional processes. An extensive review on SCF technologies applied for particle manufacturing indicates that, among others, supercritical anti-solvent (SAS, GAS, ASES, SEDS) and rapid expansion of supercritical solution (RESS, RESOLVE, RESAS, RESS-SC) are the most commonly used processes [16–22]. Generally, RESS process has advantage for preparation of nanoparticles and submicron drugs which have high solubility in SC-CO_2. In contrast, SAS processes are recommended for preparation particles which have low solubility in SC-CO_2. To this end, it is necessary to measure solubility of the desired material and analyze its behavior versus effective parameters, namely temperature and pressure. Moreover, by increasing the knowledge of the drug solubility in SCF, not only economic aspects, but also yield, particle size, shape and morphology of the product can be optimized. The main limitation of the RESS process is that the solute must have adequately high solubility in the SCF. Thakur and Gupta [23] introduced rapid expansion of a supercritical solution with the solid co-solvent (RESS-SC) process to overcome the challenges the of solubility limitation in RESS process. Later on, other researchers employed the technique to modify RESS process [18,24–26].

To the best of our knowledge, a study on the formation of LTZ

Table 1
The sources and mass fraction purity of the materials used in this paper.

Material	Source	Initial mass fraction Purity	Purification method	Final mass fraction Purity	Analysis method
Letrozole	Tofigh Darou Co.	0.99	None	0.99	GC[a]
Methanol	Merck Co.	0.999	None	0.999	GC
Menthol	Merck Co.	0.99	None	0.99	GC
CO_2	Fadak Co.	0.9999	None	0.9999	GC

[a] Gas chromatography.

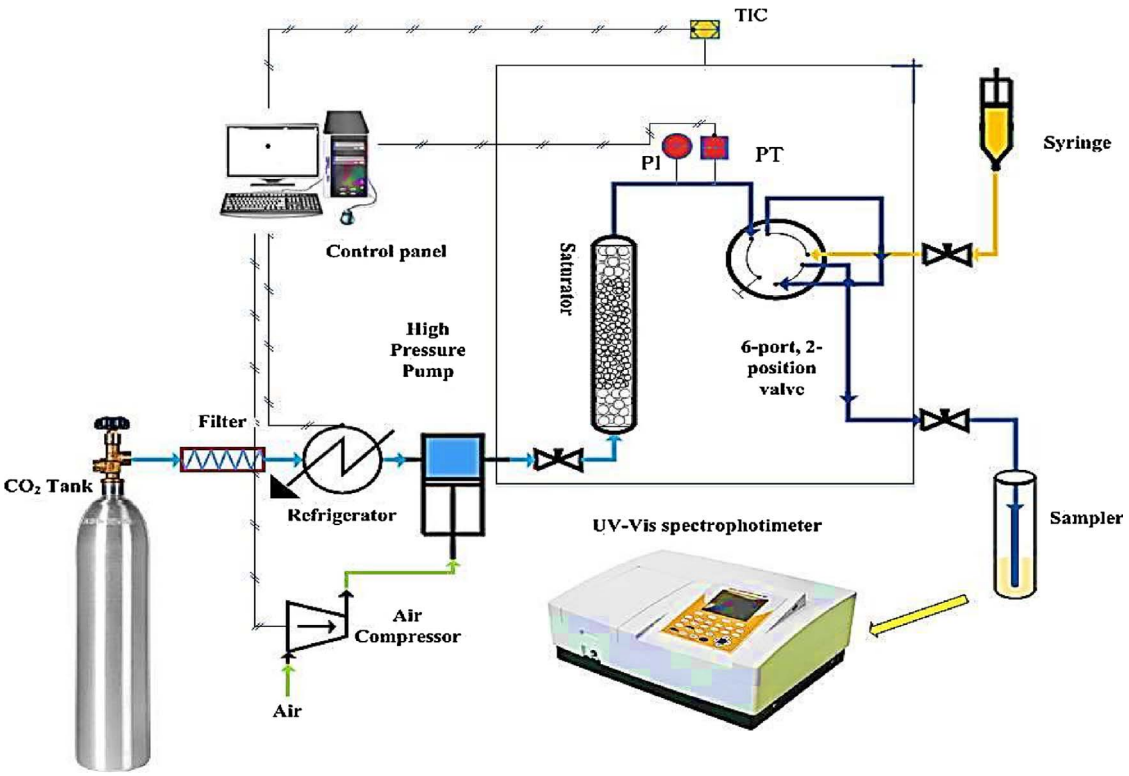

Fig 1. Schematic diagram of experimental apparatus used for measuring solubilities.

nanoparticles by SCF is yet to be reported. In this work, feasibility of the RESS-SC process when applied to reduce LTZ particles was examined. For this purpose, firstly, the static method was used to determine LTZ solubility in SCF with/without cosolvent. Afterwards, in order to optimize the conditions for the reduction of LTZ particle size, Taguchi-based design of experiments was utilized. Used to characterize processed and non-processed particles were Scanning Electron Microscopy (SEM), Dynamic Light Scattering (DLS), Differential Scanning Calorimetry (DSC), X-Ray Diffraction (XRD) and Fourier Transform Infrared Analysis (FTIR) analyses. Finally, a comparison was made in dissolution rate between non-processed and processed particles.

2. Experimental

2.1. Materials

Letrozole (CAS Number 112809-51-5) was purchased from Tofigh Darou Company (Tehran, Iran), at a minimum purity of 99%. Carbon dioxide (CO_2) (CAS Number 124-38-9) was supplied by Fadak Company (Kashan, Iran), at a minimum purity of 99.99%. These compounds were used without further purification. Menthol (CAS Number 2216-51-5) purity (Ph Eur) ≥ 99.0% and methanol (CAS Number 67-56-1) with purity (GC) ≥ 99.9% were obtained from Merck (German). Physical properties of the chemicals used in the present work are detailed in Table 1.

2.2. Solubility test apparatus

The setup illustrated in Fig. 1 is made up of the following components: carbon dioxide tank, filter, refrigerator unit, reciprocating pump equipped with an air compressor for supplying the required driving force, solubility cell, pressure gauge, digital pressure transmitter, digital thermometer, oven, microliter valve, sample collector, flow meter, piping and connections of 1/8" in size, and control panel. In this test, first, once passed through a filter of 1 μm in porosity, carbon dioxide entered the refrigerator unit where it was liquefied by decreasing its temperature from ambient to about 253 K. The liquid CO_2 at pressure of about 60 bar (pressure of CO_2 tank) was pumped to the desired pressure using the reciprocating pump. Pressure measurements were reported at an accuracy of ± 0.1 MPa by both pressure transmitter and pressure meter (WIKA, Germany). To keep the experimental temperature, the equilibrium cell was placed in a precise oven (Froilabo Model, AE-60, France) which could limit temperature instabilities within ± 0.1 K. The oven was equipped with Pt 100 poly-modulus sensors with a digital display showing regulated and real temperatures. All components of the apparatus including valves, fittings, and equilibrium cell were made of stainless steel 316 and designed for high-pressure systems operating at up to 40 MPa. Being of 70 mL in capacity, the equilibrium cell was uniformly loaded with 500 mg of LTZ alongside glass beads of 2 mm in diameter. In the cosolvent system, 1 g of menthol as cosolvent was placed in the bottom of the cell. To prevent the drug from running out of the cell, both sides of the solubility cell were fixed by a metallic sintered filter with porosity of 1 μm. In practice, SC-CO_2 was pressurized to the desired conditions and then passed into the equilibrium cell. In this research, the time to reach equilibrium state was set to 60 min, as determined to be sufficient through preliminary experiments. At the end of the static time, 600 μL of the saturated SC-CO_2 was introduced into the injection loop via a six-port, two-position valve. By switching the injection valve, the loop was depressurized into the collection vial containing a given volume of solvent (Methanol). At the end of the process, the micrometer valve was used to adjust the depressurizing process in such a way to prevent solvent dispersion. Eventually, the loop was washed with the solvent, which was collected in the collection vial. The final volume of the solution was 5 mL [14,27].

Solubilities of LTZ samples obtained under different conditions were measured by absorbency measurements at λ_{max} using a model 2100 Shimadzu UV–vis spectrophotometer equipped with quartz cells of 1 cm in pass length. Stock solutions of LTZ (100 μg mL^{-1}) were provided by dissolving appropriate amounts of solid samples in methanol. A set of standard solutions was prepared by appropriately diluting the stock

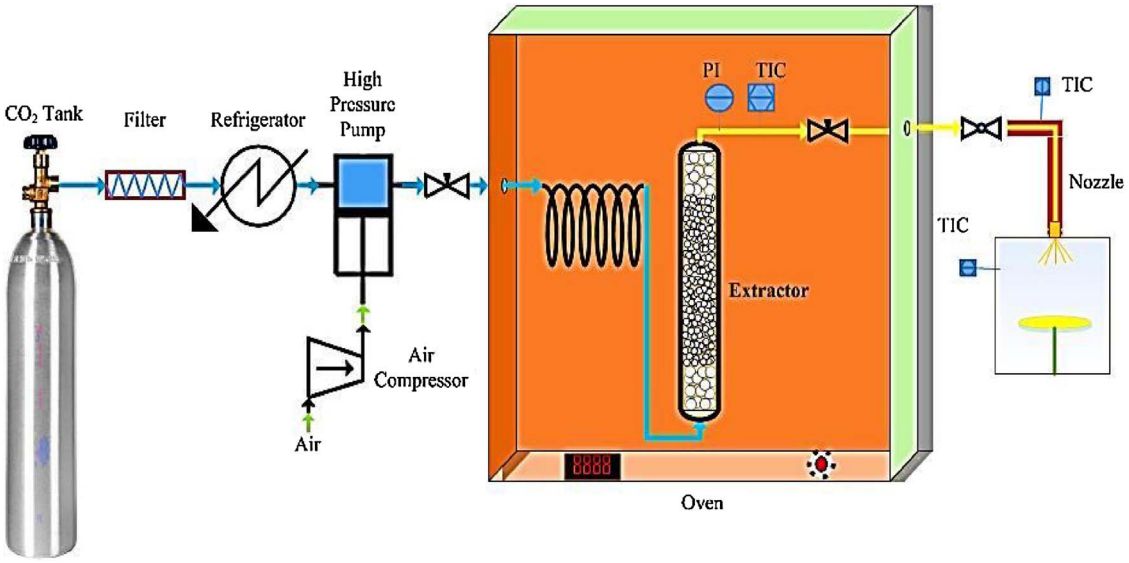

Fig. 2. Experimental apparatus for nanoparticles formation.

solutions. The calibration curves obtained (with regression coefficients of about 0.996) were used to establish the concentration of the drug in the collection vial. Quantitative analysis by UV absorption was accomplished at 240 nm for LTZ solute drug. The more details of solubility calculations was reported in our previous works [14,27].

2.3. Taguchi method

As a powerful design of experiments, the Taguchi method with orthogonal arrays was employed to optimize the parameter affecting the production of LTZ nanoparticles. This method provides a simple, efficient and systematic approach to optimize designs for performance, quality, and cost [28]. Parameter design is the key step in Taguchi method to achieve high quality without increasing the associated cost. In this study, this technique was used to identify optimal conditions for producing LTZ nanoparticles at smallest possible size. The main factors and their levels were chosen based on preliminary experiments. In this work, four factors pressure of 12–36 MPa, temperature of 318.2–348.2 K, cosolvent of 1–10 wt% and spray distance of 1–10 cm were studied at five levels. Finally, a confirmation experiment was conducted to verify the optimal process parameters obtained from the process design.

2.4. Apparatus and procedure of RESS

Schematic of the RESS setup used in this work is shown in Fig. 2. The apparatus consists of two parts, namely extraction and precipitation units. CO_2 was introduced into the extraction cell (internal volume: 70 mL) by a high-pressure reciprocating pump to reach a desired pressure (maximum 600 bar). Before that, the input carbon dioxide was cooled to around 253 K to inhibit the formation of CO_2 vapor inside the piston, thereby preventing gas lock in the high-pressure pump. The equilibrium cell was then uniformly loaded with 2 g of LTZ alongside 1 g of menthol as cosolvent. Also, glass beads of 2 mm in diameter were

Table 2
Solubility of LTZ in SC-CO_2 at various temperatures and pressures.

Temperature[a] (K)	Pressure[a] (MPa)	Density[b] (kg/m^3)	$y_2 \times 10^5$	$y_3 \times 10^3$	$y_2' \times 10^4$	e
318.2	12	659.7	0.54 ± 0.08	16.4 ± 0.34	0.41 ± 0.04	7.63
	18	790.1	0.95 ± 0.05	18.69 ± 0.58	0.68 ± 0.06	7.13
	24	850.1	1.11 ± 0.09	20.43 ± 0.47	0.76 ± 0.07	6.81
	30	890.9	1.45 ± 0.07	23.63 ± 0.61	0.91 ± 0.10	6.24
	36	922.0	1.70 ± 0.22	26.63 ± 0.41	0.97 ± 0.11	5.69
328.2	12	506.8	0.29 ± 0.07	14.7 ± 0.56	0.29 ± 0.05	9.90
	18	724.1	1.07 ± 0.11	17.34 ± 0.62	0.91 ± 0.04	8.52
	24	801.9	1.56 ± 0.06	21.09 ± 0.41	1.21 ± 0.12	7.77
	30	850.8	2.10 ± 0.18	26.36 ± 0.88	1.52 ± 0.21	7.26
	36	887.1	2.58 ± 0.17	30.82 ± 0.97	1.78 ± 0.10	6.91
338.2	12	384.1	0.21 ± 0.13	12.36 ± 0.43	0.17 ± 0.02	8.33
	18	651.1	1.41 ± 0.08	18.45 ± 0.73	1.15 ± 0.11	8.18
	24	751.1	2.98 ± 0.16	22.34 ± 0.19	1.81 ± 0.08	6.08
	30	809.6	4.56 ± 0.12	29.7 ± 0.42	2.74 ± 0.18	6.02
	36	851.3	5.11 ± 0.08	39.04 ± 0.36	2.91 ± 0.12	5.70
348.2	12	318.9	0.16 ± 0.15	12.09 ± 0.28	0.12 ± 0.03	7.81
	18	575.9	1.67 ± 0.08	19.18 ± 0.41	1.23 ± 0.08	7.34
	24	698.5	4.45 ± 0.25	24.59 ± 0.19	3.01 ± 0.21	6.84
	30	767.5	7.17 ± 0.13	32.87 ± 0.37	4.56 ± 0.42	6.37
	36	815.1	8.51 ± 0.11	43.23 ± 0.34	4.95 ± 0.21	5.81

[a] Standard uncertainty u are u(T) = 0.1 K; u(P) = ± 0.1 MPa.
[b] Data from NIST webbook (http://webbook.nist.gov/chemistry).

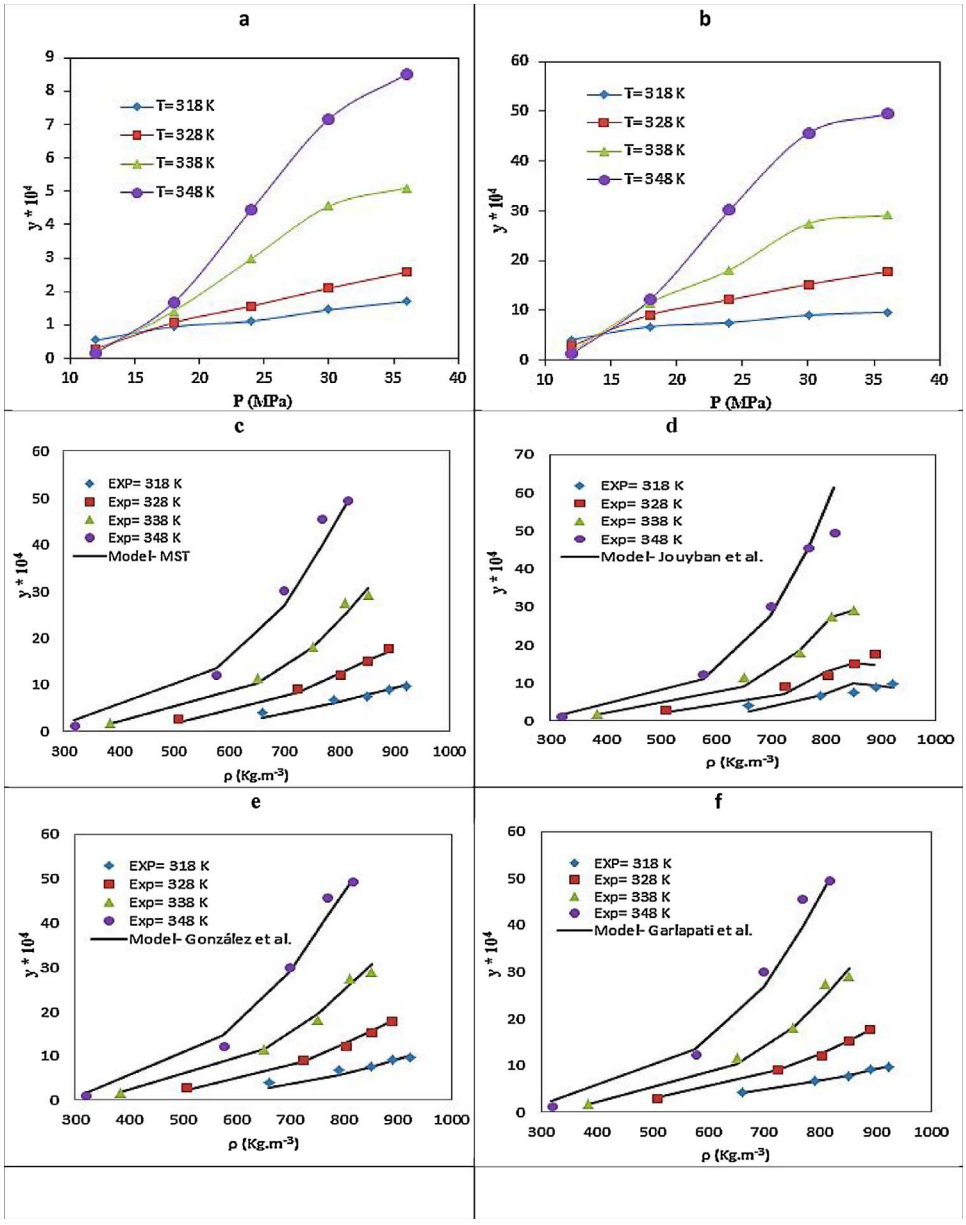

Fig. 3. Comparison of experimental and calculated solubility of LTZ based on the **a**) Binary system, **b**) Ternary system, **c**) MST, **d**) Jouyban et al. **e**) González et al. and **f**) Garlapati et al. models at various conditions.

Table 3
Summary of the density based models used in this work.

Model	Formula
MST [36]	$T\ln\left(\frac{y_2' P}{P_{ref}}\right) = a_0 + a_1\rho_1 + a_2 T + a_3 y_3$
Jouyban et al. [37]	$\ln(y_2') = a_0 + a_1 y_3 + a_2\rho_1 + a_3 P^2 + a_4 PT + \frac{a_5 T}{P} + a_6\ln(\rho_1)$
González et al. [38]	$\ln(y_2') = a_0\ln(\rho_1) + a_1\ln(y_3) + \frac{a_2}{T} + a_3$
Garlapati–Madras [39]	$\ln(y_2') = a_0 + a_1\ln(\rho_1) + a_2\rho_1 + \frac{a_3}{T} + a_4\ln(T) + a_5\ln(y_3) + a_6\ln(y_3\rho_1 T)$

Table 4
Different parameters of the LTZ – CO_2 binary system achieved various models.

Model	a_0	a_1	a_2	a_3	a_4	a_5	a_6	AARD%	R_{adj}	F-value
MST [36]	11369	3.11	29.01	2111	–	–	–	15.40	0.98	1170
Jouyban et al. [37]	−22.59	87.62	9.79E-4	−7.95E-5	1.15E-4	0.63	1.20	21.50	0.97	284
González et al. [38]	3.78	−0.037	−7692.13	−8.69	–	–	–	10.08	0.99	2100
Garlapti – Madras [39]	−14.43	5.126	−0.005	−6054.27	−2.57	−0.520	1.07	7.14	0.99	921

Table 5
Operation conditions of the RESS-SC processes and quantitative results.

Run	T (K)	P (MPa)	Cosolvent (wt.%)	Spray distance	Mean particle size (x_{50} − nm)	Predicted value (nm)
1	318.2	18	1	1	262.0	264.07
2	318.2	24	4	4	217.0	223.07
3	318.2	30	7	7	147.5	141.62
4	318.2	36	10	10	188.0	185.74
5	328.2	18	4	7	154.0	151.74
6	328.2	24	1	10	217.0	211.12
7	328.2	30	10	1	122.0	128.07
8	328.2	36	7	4	40.2	42.27
9	338.2	18	7	10	123.0	129.07
10	338.2	24	10	7	82.0	84.07
11	338.2	30	1	4	131.3	129.04
12	338.2	36	4	1	130.3	124.42
13	348.2	18	10	4	103.0	97.12
14	348.2	24	7	1	110.0	107.74
15	348.2	30	4	10	181.8	183.87
16	348.2	36	1	7	88.0	94.07
Optimum	338.2	36	7	7	19.0	20.60

used to improve saturation and distribution. Two sintered plates were used on both ends of the extraction cell to avoid any un-dissolved drug carryover with the CO_2 flow. After pumping, the carbon dioxide moved to the saturation cell was heated to the desired temperature in oven. After a static time (herein set to 60 min), the saturated LTZ-CO_2 solution was transferred into an orifice nozzle, through a pre-heated, 1/8" stainless steel tubing and fine needle valve, so as to prevent the nozzle clogging during the expansion phase. The value of volume-flow rate (2.40 L/hr) was held fixed in all experimental tests. The nozzle was situated inside the collection vessel. Most of recrystallized LTZ particles were collected in a filter within the expansion chamber. Before the tests, cosolvent was eliminated by further vacuum processing. The vacuum processing was conducted in a vacuum oven at 0.5 mbar and of 318 K until no further weight loss was observed. The elimination of solid cosolvent was confirmed by FTIR analysis. The samples were then ready for DLS and SEM analyses to monitor size and morphology of their particles. All components of the apparatus, including cooling and heating processes and the pump, were regulated by a control panel.

2.5. Particle characterization

The particles produced using RESS-SC process were characterized using Fourier Transform Infrared Analysis (FTIR), Scanning Electron Microscopy (SEM), Dynamic Light Scattering (DLS), Differential Scanning Calorimetry (DSC) and X-Ray Diffraction (XRD). SEM (TESCAN, VEGA II XMU, Czech Republic) imagery was performed to qualitatively analyze the particles for morphology, i.e. particle shape and surface characteristics. To prepare the samples for SEM image, the powder was sputter coated with gold–palladium alloy using the coating machine (BAL-TEC-SDC005, Switzerland) at room temperature for a period of 90 s. Particle size distributions of the nanoparticles were characterized using DLS method on a NANOPHOX particle sizer (Sympatec GmbH System-Partikel-Technik) equipped with a He-Ne laser (wavelength 623 nm, 10 mW) at a scattering angle of 90° as a light source. Before being analyzed with the Nanophox, LTZ (~0.01 g) was solved in deionized water (10 mL). Pre- and post-processing thermal stabilities of the APIs were studied using a DSC (DSC 404 F3 Pegasus from Netzsch; Germany). In the DSC experiments, the samples (about 5 mg/run) were heated in an aluminum standard pan under an argon gas flow of 20 mL/min and heating rate of 10 K/min. The starting and end temperatures were 30 and 230 °C, respectively. Furthermore the crystal structure, phase purity and average crystal size were investigated by powder X-ray diffractometer (Philips X'pert Pro MPD) using Cu-Kα radiation (λ = 0.154 nm) at room temperature in the 2θ range of 10–80°.

2.6. Dissolution rate

In this study, in vitro dissolution rates of the non-processed LTZ and LTZ nanoparticles were examined in a simulated intestinal fluid. For this purpose, the experimental data was measured in a 900 mL phosphate buffer solution with a pH value of 6.8. Temperature of the dissolution medium and agitator speed were maintained at 310 K and 50 rpm, respectively [29,30]. In this regard, 50 mg of each non-processed and processed LTZ sample was added separately to the dissolution medium (900 mL). For analysis, 4 mL of the liquid sample was withdrawn after 15, 20, 30, 45, 60, and 75 min using a syringe filter of 450 nm in size. Finally, the UV–vis spectrophotometer (Shimadzu, 2100), was applied to determine the concentration of the dissolved amount of LTZ in a withdrawn sample at 240 nm.

3. Results and discussion

3.1. Solubility of LTZ in SC-CO_2

Table 2 and Fig. 3a report solubilities of LTZ in pure SC-CO_2 in the pressure range 12–36 MPa and temperature range 318.2–348.2 K. Each reported data point is provided as the mean for three replicated sample measurements. It is clear that the solubility of LTZ increased with increasing pressure along each isotherm and this effect is more evident at higher temperatures, which might have caused by the combined effect of pressure and temperature on density of the solvent and solute vapor pressure. In addition, Fig. 3a describes that a crossover pressure region ranges from 16.0 to 18.0 MPa. Besides, the effect of temperature is more complicated than that of pressure. As the temperature increases, vapor pressure of LTZ increases as well, while the density of SC-CO_2 decreases, with the former leading an increase in solubility while the latter decreases the solubility. As shown in Fig. 3a, above the crossover region, the main factor affecting solubility is the vapor pressure of LTZ, which rises with temperature. Thus, the solubility increases with temperature. But, below this region, the main factor influencing the solubility is the density of SC-CO_2. The density and thus solubility decrease with increasing temperature. In brief, solubility of LTZ increases with

Table 6
Taguchi method adequacy and ANOVA analysis.

Source	Std. Dev.	R-square	Adjusted R-square	Predicted R-square	p-Value	PRESS
Model	10.38	0.9935	0.9676	0.8159	0.006	9192
Source	Sum of Squares	df	Mean Square	F-Value	Prob > F	
Model	49598.38	12	4133.20	38.37	0.0060	Significant
T	19839.20	3	6613.07	61.39	0.0034	Significant
P	5914.48	3	1971.49	18.30	0.0197	Significant
Cosolvent	14273.72	3	4757.91	44.17	0.0056	Significant
Spray distance	9570.98	3	3190.33	29.62	0.0099	Significant
Residual	323.16	3	107.72			
Cor. Total	49921.53	15				

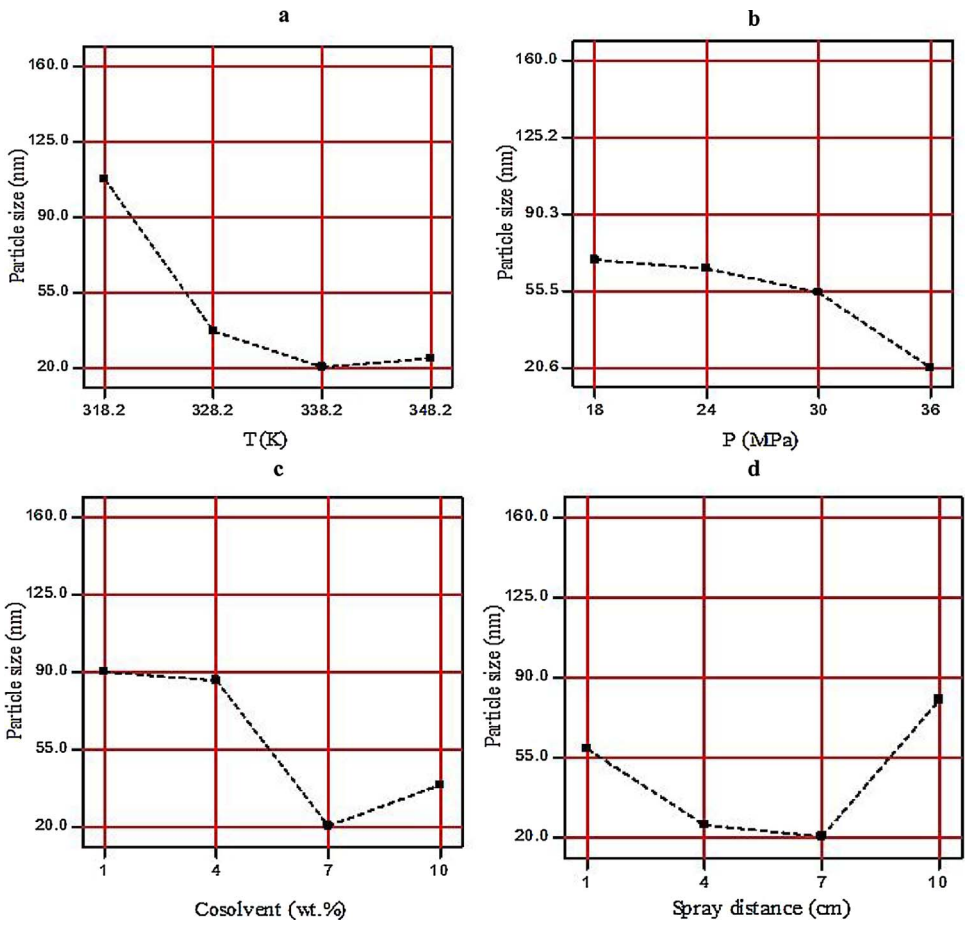

Fig. 4. Plots for the particle size as a function of: **a**) temperature; **b**) pressure; **c**) cosolvent; and **d**) spray distance. For each parameter, other parameters were constant. (temperature = 338 K, pressure = 36 MPa, cosolvent = 7% and spray distance = 7 cm).

pressure at constant temperature. This is due to the fact that as the pressure increases, generally the density increases and hence the solubility increases. Solubility of LTZ also increases with temperature at constant pressure. Even though the increase in temperature at constant pressure decreases the density, the increase in vapor pressure due to increases in temperature increases the solubility of solute. Similar results were reported by some researchers [27,31–33].

The experimental data indicates that, under the mentioned conditions, LTZ solubilities range within 10^{-6}–10^{-5} mol fraction, depending on the pressure and temperature. Recently, Hojjati et al. [34] measured solubility of LTZ in the pressure range 12–35 MPa and temperature range 308.2–348.2 K. The mean standard deviation between their experimental data and the present work was found to be 3.7%.

3.2. Solubility of LTZ in SC-CO_2 with cosolvent

In this section, the effect of a solid cosolvent (menthol) on solubility of LTZ was investigated at four temperatures (318.2, 328.2, 338.2 and 348.2 K) and pressures ranging from 12 to 36 MPa. Equilibrium solubility of menthol (y_3) and solubility LTZ in ternary system ($y_2^{'}$) in SC-CO_2 over the considered pressure and temperature ranges are tabulated in Table 2. Further presented in Table 2 was the CO_2 density, obtained from NIST chemistry web-book (http://webbook.nist.gov/chemistry/).

Table 2 and Fig. 3b show the solubility of LTZ in menthol–CO_2 system. As can be seen in Table 2, the solubility is seen to increase in presence of menthol. In order to better understand the solubility enhancement, a cosolvent effect "e" was practically defined as follows [23,35]:

$$e = \frac{y_2^{'}(P, T, y_3)}{y_2^{'}(P, T)} \tag{2}$$

The values of "*e*" are listed in Table 2, from which one can see that the solubility enhanced in presence cosolvent. The highest cosolvent effect was 9.9 folds. Furthermore, in this study, the solubility measured with cosolvents was correlated to those calculated from the equations proposed by Mendez-Santiago and Teja (MST) [36], Jouyban et al. [37], González et al. [38] and Garlapati–Madras [39] with four, four, seven and seven adjustable parameters, respectively (see Table 3). According to the number of adjustable parameters in each model and in order to provide a reliable accuracy criterion to compare the accuracy of the models possessing different numbers of curve-fitting parameters, average absolute relative deviations (AARD), adjusted correlation coefficient ($R^2_{adj.}$), and F-value were calculated [14]:

$$AARD\% = \frac{1}{N-z}\sum_{i=1}^{n}\left(\left|\frac{y_{i,cal} - y_{i,exp}}{y_{i,exp}}\right|\right) \times 100\% \tag{3}$$

$$R_{adj} = \sqrt{|R^2 - (Q(1-R^2)/(N-Q-1))|} \tag{4}$$

$$F - value = \frac{SS_R/Q}{SS_E/(N-Q-1)} = \frac{MS_R}{MS_E} \tag{5}$$

Results of the density-based models and corresponding AARD, R_{adj} and F-values are presented in Table 4. Also, the results of correlation of LTZ to the four semi-empirical models are illustrated in Fig. 3c–f. Based on statistical parameters (AARD = 7.14%, R_{adj} = 0.998 and F-value = 921), the equation proposed by Garlapati–Madras [39] was superior over other models as it was correlated well to the experimental data (Fig. 3f).

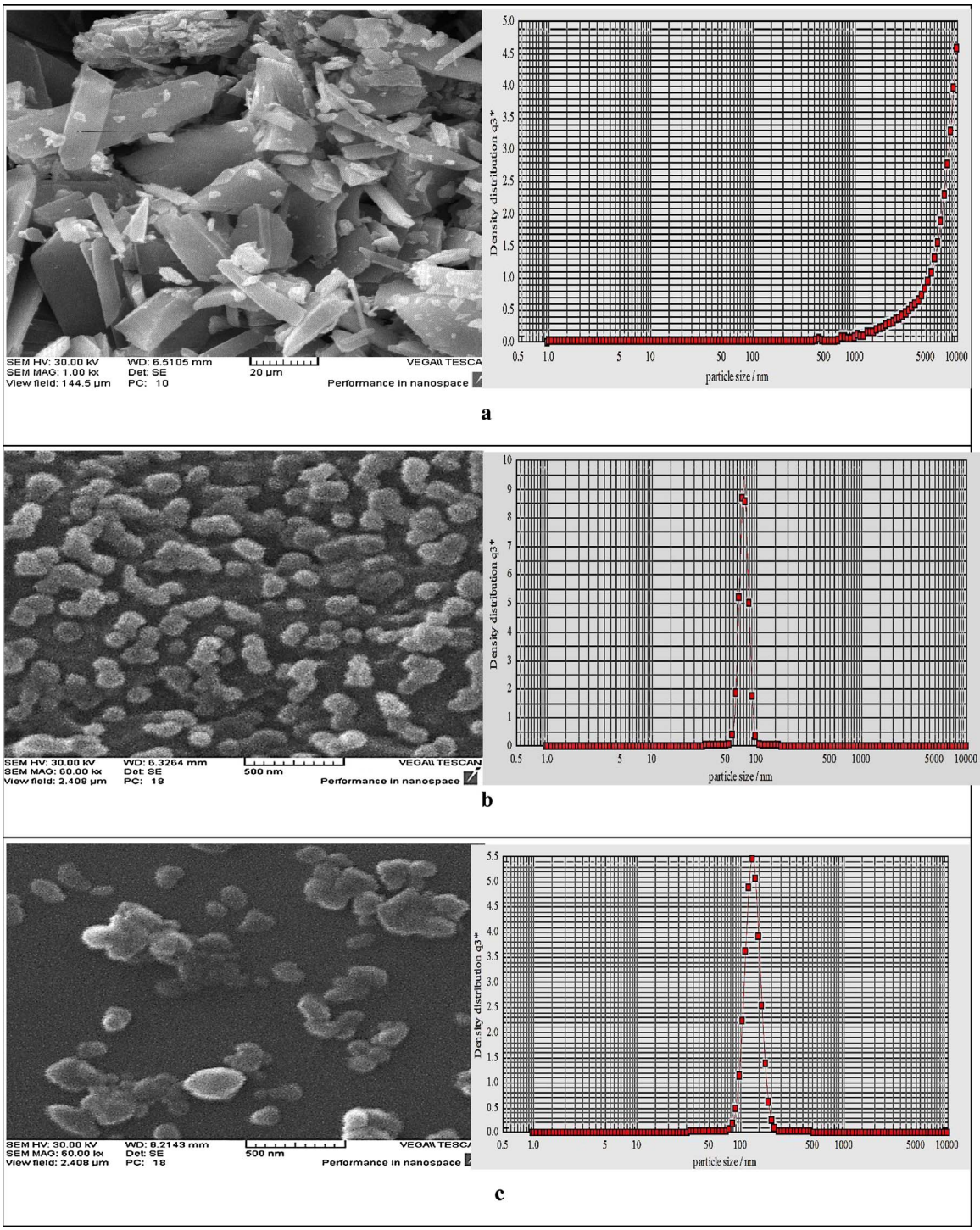

Fig. 5. SEM images for various conditions (based on Table 5): **a**) Original LTZ **b**) Run 10 **c**) Run 3.

3.3. Effect of operating conditions on particle size and particle size distribution

A Taguchi L-16 orthogonal array design was applied to investigate the influence of RESS parameters on the size and morphology of the precipitated LTZ particles. According to Table 5, the Taguchi was used for studying the four coded operating parameters including temperature (X_1), pressure (X_2), solid cosolvent (X_3) and spray distance (X_4), at four levels, namely, 1, 2, 3 and 4 within the ranges of 12–36 MPa, 318.2–348.2 K, 1–10 wt%, and 1–10 cm, respectively. It should be noted that pre-temperature, post-temperature and nozzle diameter were fixed at 353 K, 273 K and 100 µm, respectively. The experimental results obtained at different values of operating conditions and mean size of particle (x_{50}) were reported in Table 5. The values of particle size in Table 5 were achieved by DLS. Afterwards, statistical analysis was performed using Design Expert 7.0.0 software. The significance of each term was evaluated according to their corresponding probability values (*p*-values). The p-value was used as a tool to check the significance of each coefficient. A *p*-value less than 0.05 indicates that the corresponding factor has a significant influence on the process at more than 95% confidence, while *p*-values greater than 0.05 demonstrate the model insignificance. As seen in Table 6, the significant terms included

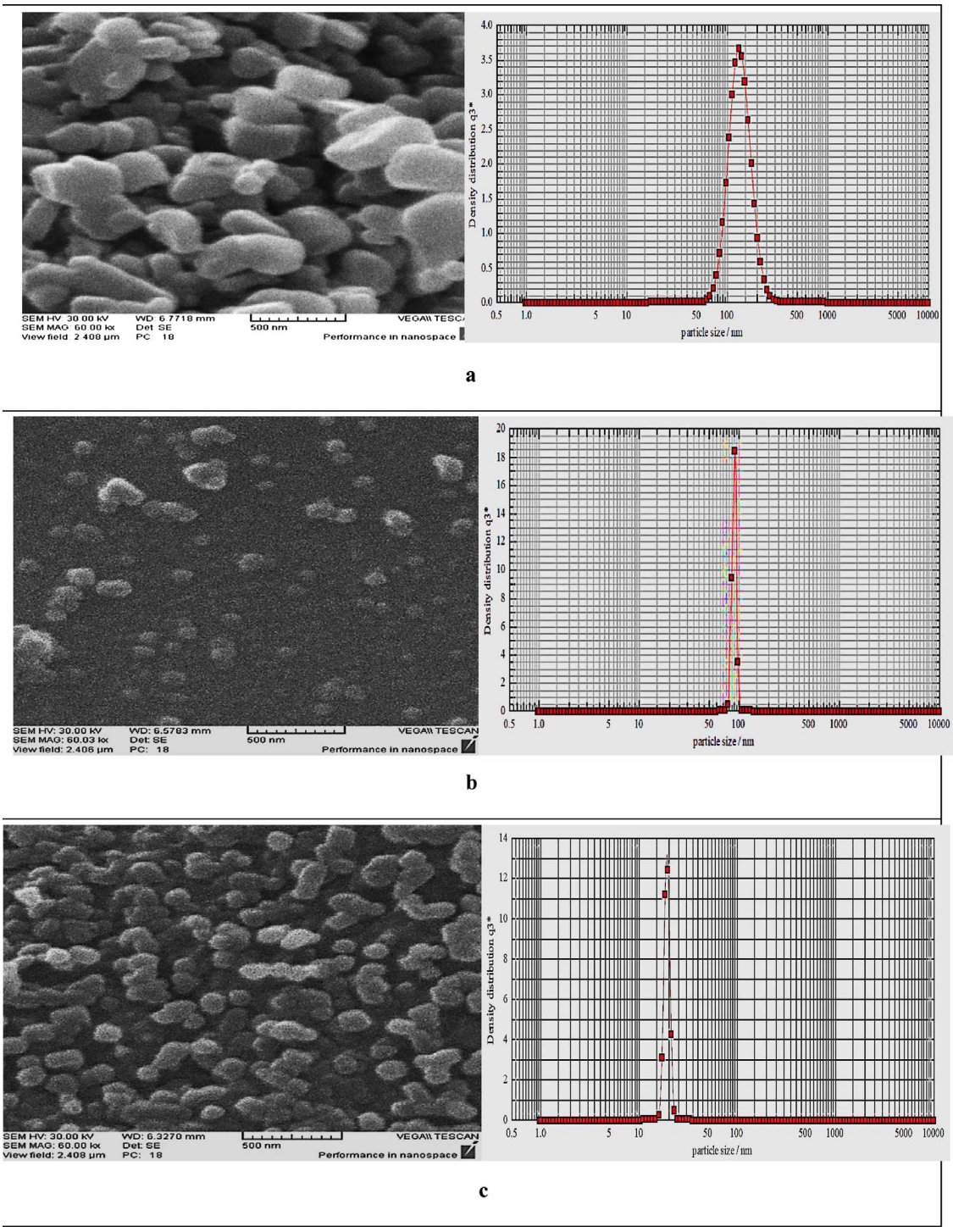

Fig. 6. SEM images for various conditions (based on Table 5): **a)** Run 6 **b)** Run 13 **c)** Optimum.

pressure, temperature, cosolvent and spray distance. Based on F-value of the parameters in Table 6, the most influential parameter in this process is temperature. Furthermore, values of determination coefficient, R^2 (R-square), adjusted R^2, and predicted R^2 were found to be 0.9935, 0.9687 and 0.8187, respectively. An adequate precision measures the signal to noise ratio, which compares the range of the predicted values at the design points to the average prediction error. A ratio greater than 4 is desirable; therefore the ratios of 23.70 indicated an adequate signal. The low value of the coefficient of variation (C.V. = 7.23) was indicative of the reliability of the experiments conducted. Hence, taking all the above facts into consideration, it can be concluded that the method is outstandingly reliable. Fig. 4a–d show the effect of process parameters on the particle size. Continuing with the results, SEM images of non-processed and some RESS-processed LTZ samples are illustrated in Figs. 5 a–c and 6 a–c . As well as, results of DLS were reported in Figs. 5 a–c and 6 a–c.

3.3.1. *Effect of temperature*

As illustrated in Fig. 4a, mean particle size decreased with increasing the temperature, and this increase was more considerable at lower pressures. As the extraction temperature was increased from 318.2 to 338.2 K, the resulted mean particle size decreased from 107.6

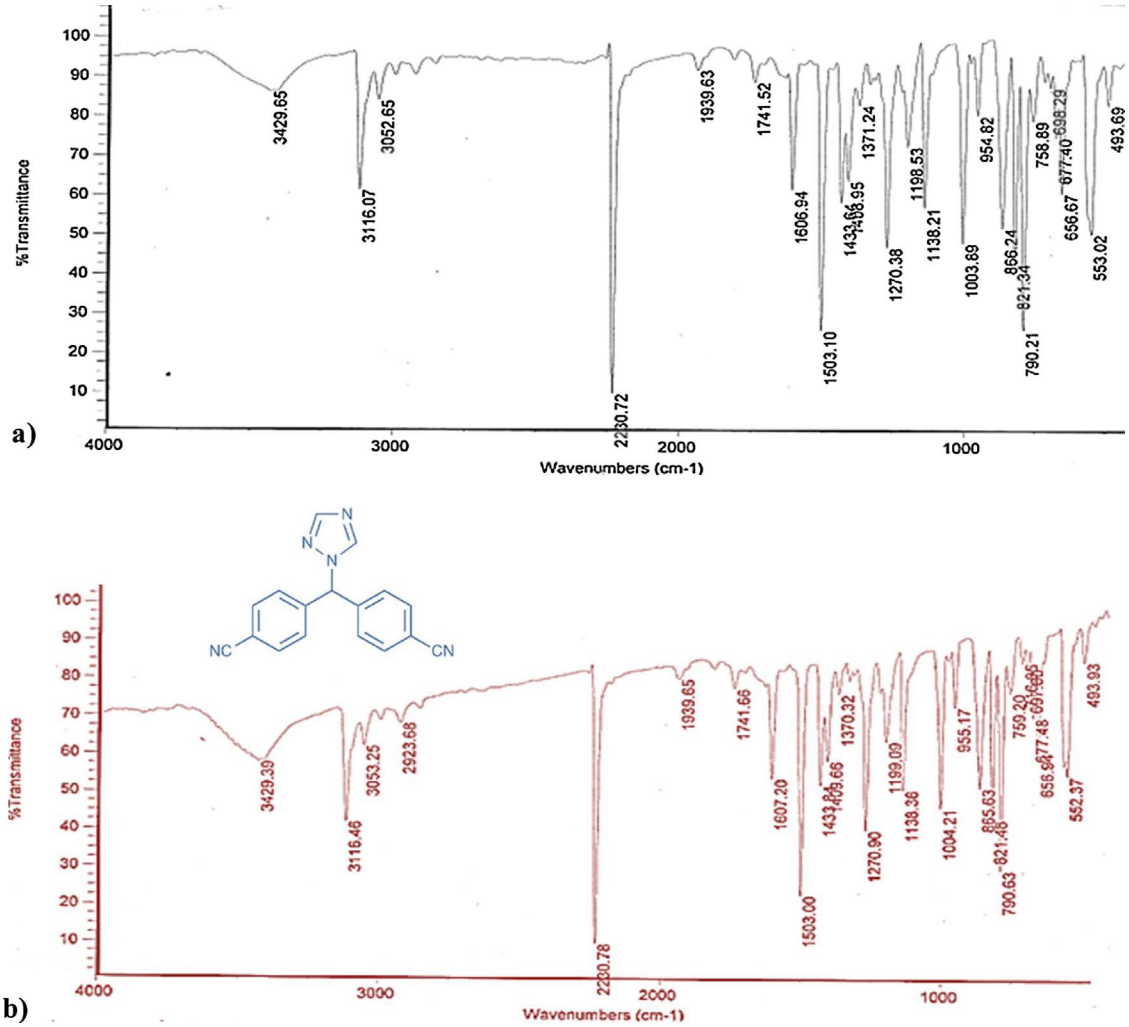

Fig. 7. Comparison of the FTIR spectrum of **a)** the original LTZ, and **b)** RESS-SC processed LTZ.

to 20.6 nm. It could be explained as follows: by increasing the temperature, the solute's volatility increased and the viscosity as well as surface tension of the LTZ decreased, favoring the RESS-SC process. This ended up with higher solubility of the solute in SC-CO_2. On the other hand, it is well-known that an increase in the extraction temperature decreases the density of SC-CO_2. However, with the samples located above the retrograded region, the elevated temperature imposes no effect on density. Fig. 4a shows that, within the pressure range of 18–36 MPa, LTZ becomes more soluble in CO_2 at higher temperatures. As mentioned previously, higher solubility and concentration contribute to larger super-saturation and nucleation rate which decrease average particle size. The trend of Fig. 4a demonstrates that, with increasing extraction temperature from 318.2 to 338.2 K, LTZ particle size decreased. This is in agreement with reports on other drugs [26,40–42]. On the other hand, obtained results show a great size reduction on the mean particle size of the precipitated particles when the extraction temperature of 318.2 and 338.2 K were used. Although the increase in temperature reduced particle size, but the higher nucleation rate at 348 K tended to increase the risk of agglomeration and coagulation of smaller particles which end up forming particles of larger size.

3.3.2. Effect of pressure

Fig. 4b shows the effect of pressure on the particle size reduction. The effect of the extraction pressure on the size and morphology of the particles was tested in the range of 18–36 MPa, while the other parameters maintained at its respective fixed optimum level. The obtained results showed that, smaller particles were formed at higher pressures. Generally, at a given temperature, solubility of LTZ in SC-CO_2 was seen to increase with pressure. An increase in the pressure increases supercritical CO_2 density which in turn enhances its solubility strength, leading to a higher super-saturation state. According to the classical theory of nucleation, at higher super-saturation, nucleation rate rises, thus decreasing average particle size [7,43]. Fixing the pre-expansion and post-expansion temperatures at 353 and 273 K, respectively, the resulted mean particle size was seen to decrease from 69.7 to 20.6 nm as extraction pressure was increased from 18 to 36 MPa. Similar results were reported by Hiendrawan et al. [44], Türk et al. [45], Yildiz et al. [46], Hazave and Esmaeilzadeh [47], and Ghoreishi et al. [40].

3.3.3. Effect of cosolvent

Fig. 4c shows the influence of value of solid cosolvent on the size of the precipitated particles while the other RESS-SC parameters including pressure (36 MPa), temperature (338 K) and spraying distance (7 cm) were kept constant. Experimental data was obtained at different cosolvent concentrations, namely 1, 4, 7 and 10 wt%. The results showed that, cosolvent had dual effects at different concentrations. In general, the concentration and nature of cosolvent affect (i.e. modify) polarity of supercritical carbon dioxide. In this case, menthol with a hydroxy (polar) group and a hydrocarbon group (non-polar) in its structure increases the solubility of letrozole in carbon dioxide. This increase occurs through the interaction between hydrogen of the hydroxy group with the pair of non-bonded electrons of the nitrile group and the

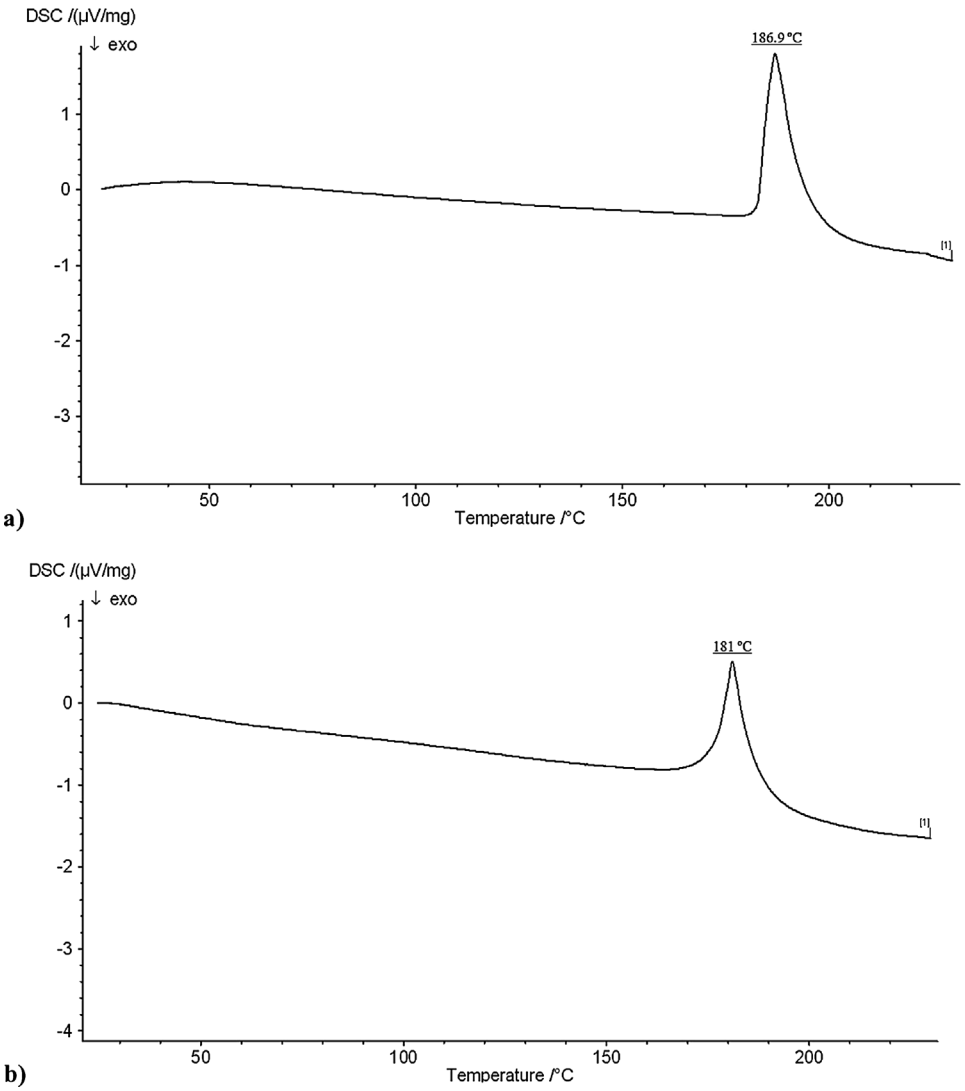

Fig. 8. DSC analysis results for LTZ before and after the RESS-SC process: **a)** the original LTZ; and **b)** RESS-SC processed LTZ, (Optimum conditions).

nitrogen present in the letrozole. The non-polar part of menthol also interacts with carbon dioxide. This result is in agreement with other researches for solute- cosolvent- SC-CO_2 system [25,48,49]. An increase in polarity of SC-CO_2 could improve the drug solubility in SC-CO_2, and at higher concentrations, cause coagulation to form larger particles. In contrast, adding cosolvent prevents particle growth in expansion zone by surrounding the drug and preventing surface to surface interaction between drug particles [24,26]. As shown in Fig. 4c, the best result for particle size was obtained at value of cosolvent 7 wt%.

3.3.4. Effect of spray distance

The effect of the spray distance (from the tip of the nozzle to the surface of the stub) on the size and shape of the precipitated particles was examined at four different spray distances (1, 4, 7 and 10 cm) at an extraction temperature of 338.2 K, pressure of 36 MPa, and solid cosolvent of 7 wt%. As can be observed in Fig. 4d, an increase in the spray distance from 1 to 7 cm caused a decrease in average particle size from 58.8 to 20.6 nm. This may be due to the fact that, as the distance increased, the jet had more time to break up the particles into smaller discrete particles; further, too short spray distances caused aggregation and particle size enlargement as the angles between the particles decrease at such distances. Some researchers have also found that, the size of precipitated drugs decrease with increasing the spraying distance [50–52]. Additionally, as shown in Fig. 4d, the spray distance may have a dual effect on particle size. Indeed, particle size decreased with increasing the spray distance to up to 7 cm and then increased as the distance was further increased to 10 cm. This dichotomy could be explained by that, with increase the spray distance, residence time of the precipitated particles increased. With longer residence time, the formed particles have enough time to grow and produce larger particles. Similar results have been reported for ibuprofen, Mefenamic acid, and salicylic acid by Kayrak et al. [53], Hazave et al. [54] and Yıldız et al. [46], respectively.

3.4. Optimum conditions

Optimum values of the process parameters were determined to obtain the smallest particle size, using Taguchi method implemented in Design Expert software. These values were determined to be the temperature of 338 K, pressure of 36 MPa, cosolvent concentration of 7 wt. % and spray distance of 7 cm. These values were predicted to give particles of 20.6 nm in size. Using Taguchi method, accuracy and validity of the optimization method were evaluated via experimentations. Accordingly, average particle size was found to be 19 nm which was very close to the estimated value (see Fig. 6c).

3.5. Characterization of Letrozole

The measured FT-IR spectrum, as KBr pellet, within the frequency range of 400–4000 cm^{-1} is shown in Fig. 7. Although the FT-IR

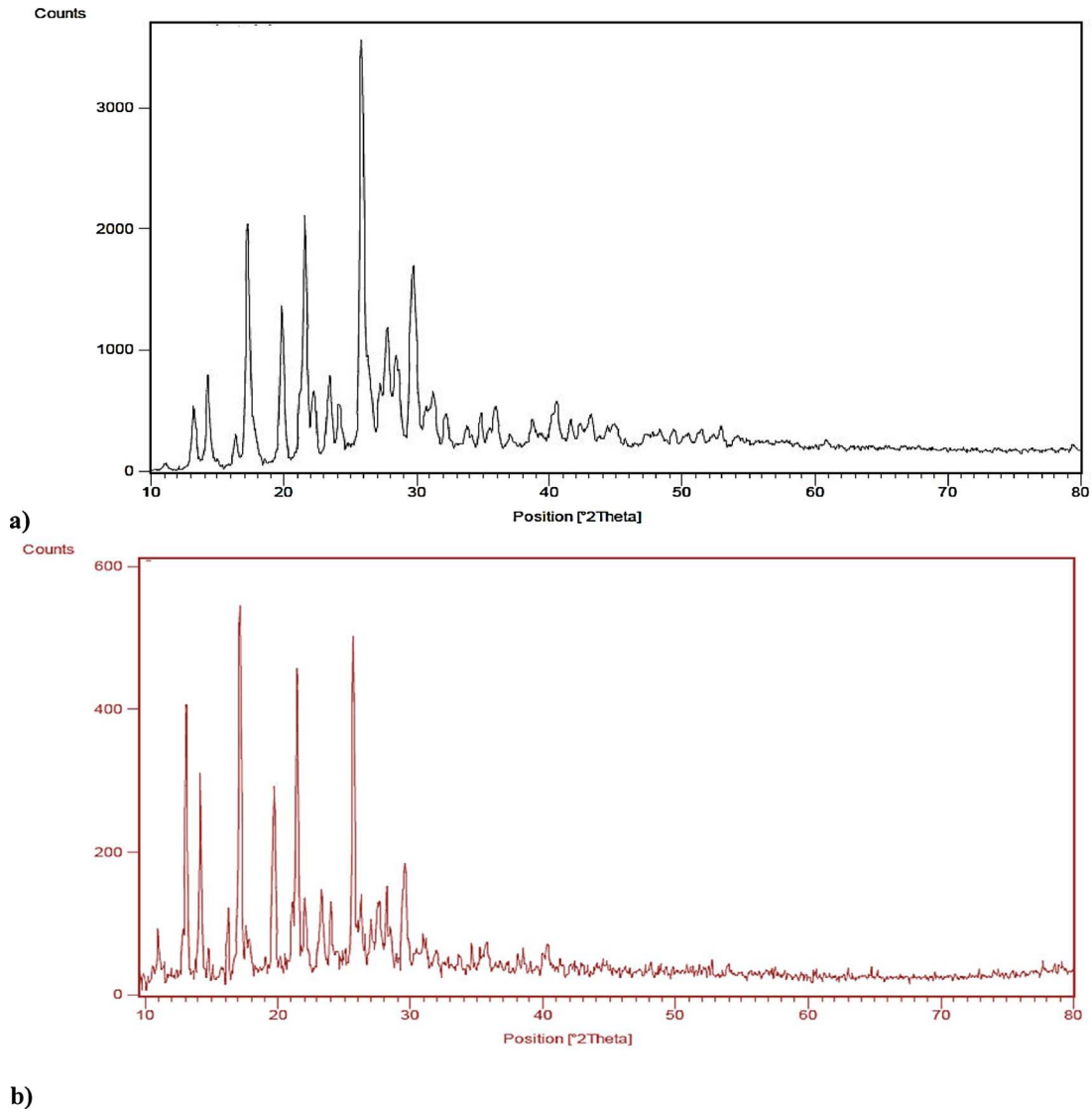

Fig. 9. XRD patterns for LTZ before and after the RESS-SC process: **a)** the original LTZ; and **b)** RESS-SC processed LTZ, (Optimum conditions).

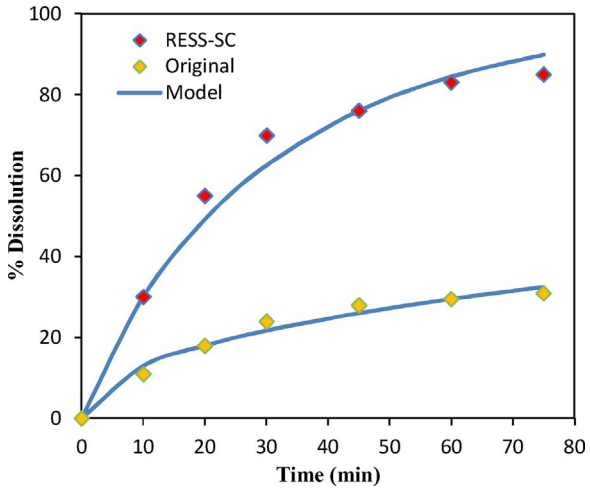

Fig. 10. Dissolution profiles for LTZ before and after the RESS-SC process (processed LTZ at optimum conditions).

Table 7
Comparison of the dissolution results for the original and processed LTZ.

Sample	a	b	k_w	f_1	f_2
Original	23.71	0.51	0.0022	–	–
RESS-SC	23.42	0.92	0.0327	184.8	17.1

spectrum shows various absorption bands, only sharp ones are considered here. In the present work, sample of un-processed and processed (optimum conditions) LTZ were characterized by the FTIR. The obtained spectra were illustrated in Fig. 7a, b. It showed that no significant differences on shape and position of the absorption peaks could be clearly observed for both. LTZ showed major peaks at 2230 cm^{-1} for C≡N stretching, 3116 cm^{-1} for sp^2 CH stretching, 698–1003 cm^{-1} for out-of-plane CH bending. In the DSC curve of the unprocessed particles, melting point is determined at 186.9 °C and for nanoparticles the peak was at 181.0 °C, which is shown in Fig. 8. This melting point depression can be investigated by the increase in thermal transfer surface and decrease in degree of crystallinity. Furthermore, The DSC results

suggest that the decrease in the enthalpy of fusion is due to the reduction in particle size and the degree in crystallinity caused by RESS [55]. Similar results were reported by Chen et al. [56], Bolten, and Türk [57] Thakur and Gupta [48], Paisana et al. [58] Ciou et al. [59] for the gemfibrozil, carbamazepine, griseofulvin, olanzapine and diuron particles respectively.

In confirming the above, XRD patterns of the unprocessed and the RESS-SC processed particles are presented in Fig. 9a, b. Based on the results of this figure, degree of crystallinity of the RESS-SC processed particles was decreased in comparison with that of the unprocessed LTZ particles. However, approximately identical structures with the lower intensity of the peaks for the RESS processed particles are indicated in Fig. 9b (at the same wavelength and diffraction angles). The reduction in the intensities may be explained due to decreasing of the crystallinity. The SEM images shown in Figs. 5, 6 reveal the significant size reduction and as modification on the morphology of the particles produced by RESS-SC. It should be emphasized that the original LTZ had an irregular shape (see Fig. 5a). In contrast, as shown in Fig. 6c, the RESS-SC process has produced a quasi-spherical particle distribution. The SEM images of original and processed particles are substantiated by DLS analysis. Based on the results obtained from DLSs, the particle size distribution of nanoparticles was 19–264 nm, which was narrower than that of original LTZ, mean of 30 μm.

3.6. In vitro dissolution rate results

The obtained results on in vitro dissolution rate of LTZ nanoparticles (under optimum conditions) demonstrated an increase in dissolution rate compared to the non-processed sample in Fig. 10. The experimental data was modeled by an empirical Weibull's model for the dissolution profile [60]. This equation is a mathematical expression for the accumulated fraction of the pharmaceutical API in a dissolution medium (m) within a specific time interval (t):

$$m = 1 - exp\left[\frac{-t^b}{a}\right] \tag{6}$$

Weibull's model illustrates the dissolved fraction of LTZ (m) in the simulated intestinal medium as a function of time, t. It has two parameters, a and b, which can be optimally fitted using dissolution data. In this case, dissolution rate coefficient (k_w) is defined as the reciprocal of the time it takes to have 63.2% of the original API dissolved. The dissolution rate coefficient was used to compare quantitative dissolution rates before and after the process. The k_w value was calculated from the Weibull's model parameters as follows [18].

$$k_w = \frac{1}{\sqrt[b]{a}} \tag{7}$$

k_w values of non-processed and processed LTZ samples were obtained from dissolution profiles (Fig. 10) as 0.0022 and 0.0327 min^{-1}, respectively, indicating a great enhancement in dissolution rate possibly due to decreased mean particle size and/or polymorph changes. Furthermore, according to U. S. FDA and European Medicines Agency (EMEA), in order to assess the dissolution of an API, dissolution profiles of RESS-SC-processed sample shall be examined by calculating so-called difference factor (f_1) and the similarity factor (f_2). Difference factor measures the difference between the two curves at each point in time, and similarity factor is calculated as follows [7,18]:

$$f_1 = \frac{\sum_{j=1}^{n} |R_j - T_j|}{\sum_{j}^{n} R_j} \times 100 \tag{8}$$

$$f_2 = 50 \times \log\left\{\left[1 + \frac{1}{n}\sum_{j=1}^{n} |R_j - T_j|^2\right]^{-0.5} \times 100\right\} \tag{9}$$

Generally, the dissolution profiles are concluded as dissimilar when f_1 values are greater than 15 and f_2 value are less than 50. As shown in Table 7, the difference factor (f_1) and similarity factor (f_2) determined from the dissolution profiles of the RESS-SC-processed LTZ were 184.80 and 17.10, respectively.

4. Conclusion

High-pressure equilibrium solubility of Letrozole in supercritical CO_2 was investigated with and without solid cosolvent in temperature range of 318.2-348.2 K and the pressure range of 12–36 MPa. The obtained mole fraction solubilities ranged from 1.6×10^{-6} to 4.48×10^{-4} for the binary system (LTZ-CO_2) and 0.12×10^{-4} to 4.95×10^{-4} for ternary system (LTZ-CO_2-menthol). With an average effect factor of 7.1, menthol was seen to significantly improve the solubility of LTZ in SC-CO_2. In addition, the data on solubility in SC-CO_2 was correlated to the models presented by González et al., Garlapati and Madras, MST, and Jouyban et al., respectively, giving AARD values of 15.4, 21.5, 10.08 and 7.14%, respectively. According to the obtained results, solubility of LTZ increased in presence of menthol, indicating that RESS-SC method can be a suitable alternative for producing and reducing LTZ nanoparticles. Rapid expansion of supercritical solution along with solid cosolvent (RESS-SC) was applied to reduce the size of Letrozole particles. The effect of RESS parameters including temperature, pressure, cosolvent and spray distance on the size and morphology of the LTZ nanoparticles were investigated using Taguchi's orthogonal array. Results of the experiments illustrated the success of RESS to produce LTZ nanoparticles of 19–264 nm in size, which is much smaller than the original LTZ. LTZ nanoparticles were characterized using FTIR, XRD, DSC, SEM and DLS analyses. The FTIR and XRD analyses demonstrated that no change has occurred in chemical structure of LTZ. Moreover, an in vitro dissolution rate test showed a significant increase in dissolution rate of nanoparticles compared to original particles. Finally, relying on the results, RESS-SC can be suggested as a favorable method for reducing the size of LTZ particles size to nano-scale, so as to raise their dissolution rate and bioavailability.

Acknowledgements

Authors would like to thank the generous financial support provided by the research deputy of University of Kashan for backing this applied, fruitful and precious plan (Grant # Pajoohaneh-1396/9). The authors would also like to thank Professor Abbas Zeraat, the Chancellor, and also Professor Mohsen Mohsen-Nia and Dr. Majid Monemzadeh, Vice-Chancellors, Dr. Hossein Tahghighi, Engineering Faculty Dean, for their helpful consolidations in providing research facilities. The authors also acknowledge Mr. Mehdi Sodeifian for his excellent technical assistance with the solubility measurement apparatus at the University of Kashan.

References

[1] H.K. Weir, M.J. Thun, B.F. Hankey, L.A. Ries, H.L. Howe, P.A. Wingo, A. Jemal, E. Ward, R.N. Anderson, B.K. Edwards, Annual report to the nation on the status of cancer, 1975–2000, featuring the uses of surveillance data for cancer prevention and control, J. Natl. Cancer Inst. 95 (2003) 1276–1299.
[2] W. Miller, Aromatase inhibitors and breast cancer, Cancer Treat. Rev. 23 (1997) 171–187.
[3] B.J. Long, D. Jelovac, V. Handratta, A. Thiantanawat, N. MacPherson, J. Ragaz, O.G. Goloubeva, A.M. Brodie, Therapeutic strategies using the aromatase inhibitor letrozole and tamoxifen in a breast cancer model, J. Natl. Cancer Inst. 96 (2004) 456–465.
[4] N. Mondal, K.K. Halder, M.M. Kamila, M.C. Debnath, T.K. Pal, S.K. Ghosal, B.R. Sarkar, S. Ganguly, Preparation, characterization, and biodistribution of letrozole loaded PLGA nanoparticles in Ehrlich Ascites tumor bearing mice, Int. J. Pharm. 397 (2010) 194–200.
[5] J. Geisler, H. Helle, D. Ekse, N.K. Duong, D.B. Evans, Y. Nordbø, T. Aas, P.E. Lønning, Letrozole is superior to anastrozole in suppressing breast cancer tissue and plasma estrogen levels, Clin. Cancer Res. 14 (2008) 6330–6335.
[6] Y. Tozuka, Y. Miyazaki, H. Takeuchi, A combinational supercritical CO 2 system for nanoparticle preparation of indomethacin, Int. J. Pharm. 386 (2010) 243–248.
[7] A. Keshavarz, J. Karimi-Sabet, A. Fattahi, A. Golzary, M. Rafiee-Tehrani,

F.A. Dorkoosh, Preparation and characterization of raloxifene nanoparticles using rapid expansion of supercritical solution (RESS), J. Supercrit. Fluids 63 (2012) 169–179.
[8] M. Türk, D. Bolten, Formation of submicron poorly water-soluble drugs by rapid expansion of supercritical solution (RESS): results for naproxen, J. Supercrit. Fluids 55 (2010) 778–785.
[9] A. Shariati, C.J. Peters, Recent developments in particle design using supercritical fluids, Curr. Opin. Solid State Mater. Sci. 7 (2003) 371–383.
[10] Y. Hakuta, H. Hayashi, K. Arai, Fine particle formation using supercritical fluids, Curr. Opin. Solid State Mater. Sci. 7 (2003) 341–351.
[11] G. Sodeifian, S.A. Sajadian, N.S. Ardestani, Optimization of essential oil extraction from Launaea acanthodes Boiss: utilization of supercritical carbon dioxide and cosolvent, J. Supercrit. Fluids 116 (2016) 46–56.
[12] G. Sodeifian, S.A. Sajadian, N.S. Ardestani, Supercritical fluid extraction of omega-3 from Dracocephalum kotschyi seed oil: process optimization and oil properties, J. Supercrit. Fluids 119 (2017) 139–149.
[13] G. Sodeifian, S.A. Sajadian, N.S. Ardestani, Extraction of Dracocephalum kotschyi Boiss using supercritical carbon dioxide: experimental and optimization, J. Supercrit. Fluids 107 (2016) 137–144.
[14] G. Sodeifian, S.A. Sajadian, N.S. Ardestani, Determination of solubility of aprepitant (an antiemetic drug for chemotherapy) in supercritical carbon dioxide: empirical and thermodynamic models, J. Supercrit. Fluids 128 (2017) 102–111.
[15] G. Sodeifian, N.S. Ardestani, S.A. Sajadian, S. Ghorbandoost, Application of supercritical carbon dioxide to extract essential oil from Cleome coluteoides Boiss: experimental, response surface and grey wolf optimization methodology, J. Supercrit. Fluids 114 (2016) 55–63.
[16] M.J. Cocero, Á. Martín, F. Mattea, S. Varona, Encapsulation and co-precipitation processes with supercritical fluids: fundamentals and applications, J. Supercrit. Fluids 47 (2009) 546–555.
[17] E. Reverchon, R. Adami, Nanomaterials and supercritical fluids, J. Supercrit. Fluids 37 (2006) 1–22.
[18] P.-C. Lin, C.-S. Su, M. Tang, Y.-P. Chen, Micronization of tolbutamide using rapid expansion of supercritical solution with solid co-solvent (RESS-SC) process, Res. Chem. Intermed. 37 (2011) 153–163.
[19] S.-D. Yeo, E. Kiran, Formation of polymer particles with supercritical fluids: a review, J. Supercrit. Fluids 34 (2005) 287–308.
[20] E. Reverchon, R. Adami, S. Cardea, G. Della Porta, Supercritical fluids processing of polymers for pharmaceutical and medical applications, J. Supercrit. Fluids 47 (2009) 484–492.
[21] P. Gosselin, R. Thibert, M. Preda, J. McMullen, Polymorphic properties of micronized carbamazepine produced by RESS, Int. J. Pharm. 252 (2003) 225–233.
[22] N. Esfandiari, Production of micro and nano particles of pharmaceutical by supercritical carbon dioxide, J. Supercrit. Fluids 100 (2015) 129–141.
[23] R. Thakur, R.B. Gupta, Rapid expansion of supercritical solution with solid cosolvent (RESS- SC) process: formation of griseofulvin nanoparticles, Ind. Eng. Chem. Res. 44 (2005) 7380–7387.
[24] H. Uchida, M. Nishijima, K. Sano, K. Demoto, J. Sakabe, Y. Shimoyama, Production of theophylline nanoparticles using rapid expansion of supercritical solutions with a solid cosolvent (RESS-SC) technique, J. Supercrit. Fluids 105 (2015) 128–135.
[25] R. Thakur, R.B. Gupta, Formation of phenytoin nanoparticles using rapid expansion of supercritical solution with solid cosolvent (RESS-SC) process, Int. J. Pharm. 308 (2006) 190–199.
[26] M. Samei, A. Vatanara, S. Fatemi, A.R. Najafabadi, Process variables in the formation of nanoparticles of megestrol acetate through rapid expansion of supercritical CO 2, J. Supercrit. Fluids 70 (2012) 1–7.
[27] G. Sodeifian, S.A. Sajadian, F. Razmimanesh, Solubility of an antiarrhythmic drug (amiodarone hydrochloride) in supercritical carbon dioxide: experimental and modeling, Fluid Phase Equilib. (2017).
[28] G. Sodeifian, K. Ansari, Optimization of Ferulago Angulata oil extraction with supercritical carbon dioxide, J. Supercrit. Fluids 57 (2011) 38–43.
[29] P.-C. Lin, C.-S. Su, M. Tang, Y.-P. Chen, Micronization of ethosuximide using the rapid expansion of supercritical solution (RESS) process, J. Supercrit. Fluids 72 (2012) 84–89.
[30] A. Fattahi, J. Karimi-Sabet, A. Keshavarz, A. Golzary, M. Rafiee-Tehrani, F.A. Dorkoosh, Preparation and characterization of simvastatin nanoparticles using rapid expansion of supercritical solution (RESS) with trifluoromethane, J. Supercrit. Fluids 107 (2016) 469–478.
[31] N. Vedaraman, G. Brunner, C.S. Kannan, B. Ramabrahmam, P. Rao, Solubility of N-CBZ derivatised amino acids in supercritical carbon dioxide, J. Supercrit. Fluids 30 (2004) 119–125.
[32] Y. Yamini, M. Moradi, M. Hojjati, F. Nourmohammadian, A. Saleh, Solubilities of some disperse yellow dyes in supercritical CO2, J. Chem. Eng. Data 55 (2010) 3896–3900.
[33] H. Asiabi, Y. Yamini, F. Latifeh, A. Vatanara, Solubilities of four macrolide antibiotics in supercritical carbon dioxide and their correlations using semi-empirical models, J. Supercrit. Fluids 104 (2015) 62–69.
[34] M. Hojjati, A. Vatanara, Y. Yamini, M. Moradi, A.R. Najafabadi, Supercritical CO 2 and highly selective aromatase inhibitors: experimental solubility and empirical data correlation, J. Supercrit. Fluids 50 (2009) 203–209.
[35] Z. Huang, S. Kawi, Y. Chiew, Solubility of cholesterol and its esters in supercritical carbon dioxide with and without cosolvents, J. Supercrit. Fluids 30 (2004) 25–39.
[36] J. Méndez-Santiago, A.S. Teja, The solubility of solids in supercritical fluids, Fluid Phase Equilib. 158 (1999) 501–510.
[37] A. Jouyban, M. Rehman, B.Y. Shekunov, H.K. Chan, B.J. Clark, P. York, Solubility prediction in supercritical CO2 using minimum number of experiments, J. Pharm. Sci. 91 (2002) 1287–1295.
[38] J.C. González, M.R. Vieytes, A.M. Botana, J.M. Vieites, L.M. Botana, Modified mass action law-based model to correlate the solubility of solids and liquids in entrained supercritical carbon dioxide, J. Chromatogr. A 910 (2001) 119–125.
[39] C. Garlapati, G. Madras, New empirical expressions to correlate solubilities of solids in supercritical carbon dioxide, Thermochim. Acta 500 (2010) 123–127.
[40] S. Ghoreishi, A. Hedayati, M. Kordnejad, Micronization of chitosan via rapid expansion of supercritical solution, J. Supercrit. Fluids 111 (2016) 162–170.
[41] Z. Huang, G.-B. Sun, Y.C. Chiew, S. Kawi, Formation of ultrafine aspirin particles through rapid expansion of supercritical solutions (RESS), Adv. Powder Technol. 160 (2005) 127–134.
[42] J.-T. Kim, H.-L. Kim, C.-S. Ju, Micronization and characterization of drug substances by RESS with supercritical CO 2, Korean J. Chem. Eng. 27 (2010) 1139–1144.
[43] A.Z. Hezave, F. Esmaeilzadeh, Fabrication of micron level particles of amoxicillin by rapid expansion of supercritical solution, J. Dispers. Sci. Technol. 33 (2012) 1419–1428.
[44] S. Hiendrawan, B. Veriansyah, R.R. Tjandrawinata, Micronization of fenofibrate by rapid expansion of supercritical solution, J. Ind. Eng. Chem. 20 (2014) 54–60.
[45] M. Türk, P. Hils, B. Helfgen, K. Schaber, H.-J. Martin, M.A. Wahl, Micronization of pharmaceutical substances by the rapid expansion of supercritical solutions (RESS): a promising method to improve bioavailability of poorly soluble pharmaceutical agents, J. Supercrit. Fluids 22 (2002) 75–84.
[46] N. Yildiz, Ş. Tuna, O. Döker, A. Çalimli, Micronization of salicylic acid and taxol (paclitaxel) by rapid expansion of supercritical fluids (RESS), J. Supercrit. Fluids 41 (2007) 440–451.
[47] A.Z. Hezave, F. Esmaeilzadeh, Crystallization of micro particles of sulindac using rapid expansion of supercritical solution, J. Cryst. Growth 312 (2010) 3373–3383.
[48] R. Thakur, R.B. Gupta, Rapid expansion of supercritical solution with solid cosolvent (RESS-SC) process: formation of griseofulvin nanoparticles, Ind. Eng. Chem. Res. 44 (2005) 7380–7387.
[49] H. Uchida, M. Nishijima, K. Sano, K. Demoto, J. Sakabe, Y. Shimoyama, Production of theophylline nanoparticles using rapid expansion of supercritical solutions with a solid cosolvent (RESS-SC) technique, J. Supercrit. Fluids 105 (2015) 128–135.
[50] M. Charoenchaitrakool, F. Dehghani, N. Foster, H. Chan, Micronization by rapid expansion of supercritical solutions to enhance the dissolution rates of poorly water-soluble pharmaceuticals, Ind. Eng. Chem. Res. 39 (2000) 4794–4802.
[51] J.-H. Yim, W.-S. Kim, J.S. Lim, Recrystallization of adefovir dipivoxil particles using the rapid expansion of supercritical solutions (RESS) process, J. Supercrit. Fluids 82 (2013) 168–176.
[52] C. Atila, N. Yıldız, A. Çalımlı, Particle size design of digitoxin in supercritical fluids, J. Supercrit. Fluids 51 (2010) 404–411.
[53] D. Kayrak, U. Akman, Ö. Hortaçsu, Micronization of ibuprofen by RESS, J. Supercrit. Fluids 26 (2003) 17–31.
[54] A.Z. Hezave, F. Esmaeilzadeh, Micronization of drug particles via RESS process, J. Supercrit. Fluids 52 (2010) 84–98.
[55] M. Türk, D. Bolten, Polymorphic properties of micronized mefenamic acid nabumetone, paracetamol and tolbutamide produced by rapid expansion of supercritical solutions (RESS), J. Supercrit. Fluids 116 (2016) 239–250.
[56] Y.-M. Chen, P.-C. Lin, M. Tang, Y.-P. Chen, Solid solubility of antilipemic agents and micronization of gemfibrozil in supercritical carbon dioxide, J. Supercrit. Fluids 52 (2010) 175–182.
[57] D. Bolten, M. Türk, Micronisation of carbamazepine through rapid expansion of supercritical solution (RESS), J. Supercrit. Fluids 62 (2012) 32–40.
[58] M.C. Paisana, K.C. Müllers, M.A. Wahl, J.F. Pinto, Production and stabilization of olanzapine nanoparticles by rapid expansion of supercritical solutions (RESS), J. Supercrit. Fluids 109 (2016) 124–133.
[59] J.-L. Ciou, C.-S. Su, Measurement of solid solubilities of diuron in supercritical carbon dioxide and analysis of recrystallization by using the rapid expansion of supercritical solutions process, J. Supercrit. Fluids 107 (2016) 753–759.
[60] P. Costa, J.M.S. Lobo, Modeling and comparison of dissolution profiles, Eur. J. Pharm. Sci. 13 (2001) 123–133.